

Ultrafast two-dimensional x-ray imager with temporal fiducial pulses for laser-produced plasmas

Zheng-Dong Liu(刘正东), Jia-Yong Zhong(仲佳勇), Xiao-Hui Yuan(远晓辉), Ya-Peng Zhang(张雅芃), Jia-Wen Yao(姚嘉文), Zuo-Lin Ma(马作霖), Xiang-Yan Xu(徐向晏), Yan-Hua Xue(薛彦华), Zhe Zhang(张喆), Da-Wei Yuan(袁大伟), Min-Rui Zhang(张敏睿), Bing-Jun Li(李炳均), Hao-Chen Gu(谷昊琛), Yu Dai(戴羽), Cheng-Long Zhang(张成龙), Yu-Feng Dong(董玉峰), Peng Zhou(周鹏), Xin-Jie Ma(马鑫杰), Yun-Feng Ma(马云峰), Xue-Jie Bai(白雪洁), Gao-Yang Liu(刘高扬), Jin-Shou Tian(田进寿), Gang Zhao(赵刚), and Jie Zhang(张杰)
Citation: Chin. Phys. B, 2023, 32 (**11**): 110702. DOI: 10.1088/1674-1056/ace766
Journal homepage: http://cpb.iphy.ac.cn; http://iopscience.iop.org/cpb

What follows is a list of articles you may be interested in

Characterization and application in XRF of HfO_2-coated glass monocapillary based on atomic layer deposition

Yan-Li Li(李艳丽), Ya-Bing Wang(王亚冰), Wei-Er Lu(卢维尔), Xiang-Dong Kong(孔祥东), Li Han(韩立), and Hui-Bin Zhao(赵慧斌)
Chin. Phys. B, 2021, 30 (**5**): 050703. DOI: 10.1088/1674-1056/abcfa2

Broadband time-resolved elliptical crystal spectrometer for X-ray spectroscopic measurements in laser-produced plasmas

Wang Rui-Rong (王瑞荣), Jia Guo (贾果), Fang Zhi-Heng (方智恒), Wang Wei (王伟), Meng Xiang-Fu (孟祥富), Xie Zhi-Yong (谢志勇), Zhang Fan (张帆)
Chin. Phys. B, 2014, 23 (**11**): 113201. DOI: 10.1088/1674-1056/23/11/113201

Single order soft X-ray diffraction with quasi-random radius pinhole array spectroscopic photon sieves

Zhang Qiang-Qiang (张强强), Wei Lai (魏来), Yang Zu-Hua (杨祖华), Qian Feng (钱凤), Fan Quan-Ping (范全平), Zhang Bo (张博), Gu Yu-Qiu (谷渝秋), Cao Lei-Feng (曹磊峰)
Chin. Phys. B, 2014, 23 (**4**): 044215. DOI: 10.1088/1674-1056/23/4/044215

Measurement of inner surface roughness of capillary by an x-ray reflectivity method

Li Yu-De(李玉德),Lin Xiao-Yan(林晓燕),Tan Zhi-Yuan(谭植元), Sun Tian-Xi(孙天希),and Liu Zhi-Guo(刘志国)
Chin. Phys. B, 2011, 20 (**4**): 040702. DOI: 10.1088/1674-1056/20/4/040702

INSTRUMENTATION AND MEASUREMENT

Ultrafast two-dimensional x-ray imager with temporal fiducial pulses for laser-produced plasmas

Zheng-Dong Liu(刘正东)[1,2], Jia-Yong Zhong(仲佳勇)[1,2,6,†], Xiao-Hui Yuan(远晓辉)[5,6], Ya-Peng Zhang(张雅芃)[1,2], Jia-Wen Yao(姚嘉文)[1,2], Zuo-Lin Ma(马作霖)[1,2], Xiang-Yan Xu(徐向晏)[3], Yan-Hua Xue(薛彦华)[3], Zhe Zhang(张喆)[4,6,11], Da-Wei Yuan(袁大伟)[2,7], Min-Rui Zhang(张敏睿)[3], Bing-Jun Li(李炳均)[9], Hao-Chen Gu(谷昊琛)[4,12], Yu Dai(戴羽)[4,12], Cheng-Long Zhang(张成龙)[8,4], Yu-Feng Dong(董玉峰)[4,12], Peng Zhou(周鹏)[5,6], Xin-Jie Ma(马鑫杰)[9], Yun-Feng Ma(马云峰)[9], Xue-Jie Bai(白雪洁)[9], Gao-Yang Liu(刘高扬)[10], Jin-Shou Tian(田进寿)[3], Gang Zhao(赵刚)[7], and Jie Zhang(张杰)[4,5,6]

[1] *Department of Astronomy, Beijing Normal University, Beijing* 100875, *China*
[2] *Institute for Frontiers in Astronomy and Astrophysics, Beijing Normal University, Beijing* 102206, *China*
[3] *Xi'an Institute of Optics and Precision Mechanics, Chinese Academy of Sciences, Xi'an* 710119, *China*
[4] *Beijing National Laboratory for Condensed Matter Physics, Institute of Physics, Chinese Academy of Sciences, Beijing* 100190, *China*
[5] *Key Laboratory for Laser Plasmas (MoE) and School of Physics and Astronomy, Shanghai Jiao Tong University, Shanghai* 200240, *China*
[6] *Collaborative Innovation Center of IFSA (CICIFSA), Shanghai Jiao Tong University, Shanghai* 200240, *China*
[7] *Key Laboratory of Optical Astronomy, National Astronomical Observatories, Chinese Academy of Sciences, Beijing* 100101, *China*
[8] *State Key Laboratory for Geomechanics and Deep Underground Engineering, China University of Mining and Technology, Beijing* 100083, *China*
[9] *School of Nuclear Science and Technology, Xi'an Jiaotong University, Xi'an* 710049, *China*
[10] *School of Sciences, Harbin Institute of Technology at Weihai, Weihai* 264209, *China*
[11] *Songshan Lake Materials Laboratory, Guangdong* 523808, *China*
[12] *School of Physical Sciences, University of Chinese Academy of Sciences, Beijing* 100049, *China*

(Received 13 May 2023; revised manuscript received 4 July 2023; accepted manuscript online 14 July 2023)

It is challenging to make an ultrafast diagnosis of the temporal evolution of small and short-lived plasma in two dimensions. To overcome this difficulty, we have developed a well-timed diagnostic utilizing an x-ray streak camera equipped with a row of multi-pinhole arrays. By processing multiple sets of one-dimensional streaked image data acquired from various pinholes, we are capable of reconstructing high-resolution two-dimensional images with a temporal resolution of 38 ps and a spatial resolution of 18 μm. The temporal fiducial pulses accessed from external sources can advance the precise timing and accurately determine the arrival time of the laser. Moreover, it can correct the nonlinear sweeping speed of the streak camera. The effectiveness of this diagnostic has been successfully verified at the Shenguang-II laser facility, providing an indispensable tool for observing complex physical phenomena, such as the implosion process of laser-fusion experiments.

Keywords: ultrafast diagnosis, double-cone ignition, x-ray streak camera, pinhole array, temporal fiducial pulses

PACS: 07.85.–m, 29.90.+r, 28.41.Rc, 28.52.Cx **DOI:** 10.1088/1674-1056/ace766

1. Introduction

Ultrafast x-ray imaging is crucial for diagnosing small and short-lived plasmas, such as imploded and stagnated plasma in the inertial confinement fusion (ICF) scheme.[1] These processes occur on temporal and spatial scales of several hundred picoseconds or micrometers, requiring temporal and spatial resolutions of a few tens of picoseconds and a few microns, respectively.[2] While gated x-ray framing cameras provide excellent two-dimensional (2D) spatial-intensity information, their temporal resolution is restricted to 80 ps, accompanied by a limited number of frames.[3,4] In contrast, an x-ray streak camera (XSC) can achieve a higher temporal resolution of better than 10 ps,[5] but it is only capable of capturing one-dimensional spatial information. To overcome those limitations, in 1990, Choi *et al.*[6] applied a streaked multi-pinhole camera technique to record plasma with continuous time resolution and 2D space resolution produced by plasma-focusing devices. In 1992, Landen applied this method to the observation of laser-generated plasma.[7] Furthermore, Shiraga *et al.*[8–10] developed and utilized a multi-imaging XSC (MIXS) to observe the temporal and spatial evolution of imploding core plasma in laser-fusion targets.

MIXS is commonly utilized in fast ignition[11] and double-cone ignition (DCI) experiments[12] to track the 2D evolution of plasma spontaneous radiation and provide accurate heating time for subsequent injection of fast electrons. Nevertheless, due to the limited field of view, the traditional MIXS is unable to capture simultaneous images of both the

†Corresponding author. E-mail: jyzhong@bnu.edu.cn
© 2023 Chinese Physical Society and IOP Publishing Ltd

coronal and collision regions in a DCI experiment. Therefore, it is impossible to determine the laser end time by the spontaneous light of the coronal plasma. As a result, accurate physical information and diagnostic moments cannot be provided for other diagnoses during the experiment.

In this paper, we report the development and optimization of a new ultrafast x-ray imaging technology, multi-image with an XSC with temporal fiducial pulses (MIXS-F), and we present experimental results using this technique to visualize small, short-lived plasma evolution in two dimensions. The timing fiducial pulses can accurately determine the laser time and correct the sweeping nonlinearity of XSC. We have performed an experiment on the Shenguang-II (SG-II) laser facility to test the system, and we reconstructed the time-dependent 2D x-ray images with temporal and spatial resolutions of about 38 ps and 18 μm, respectively.

2. MIXS with temporal fiducial pulses

MIXS-F is composed of a pinhole array, an XSC, and a set of temporal fiducial pulses. The schematic diagram of its equipment and the solid diagram are shown in Fig. 1.

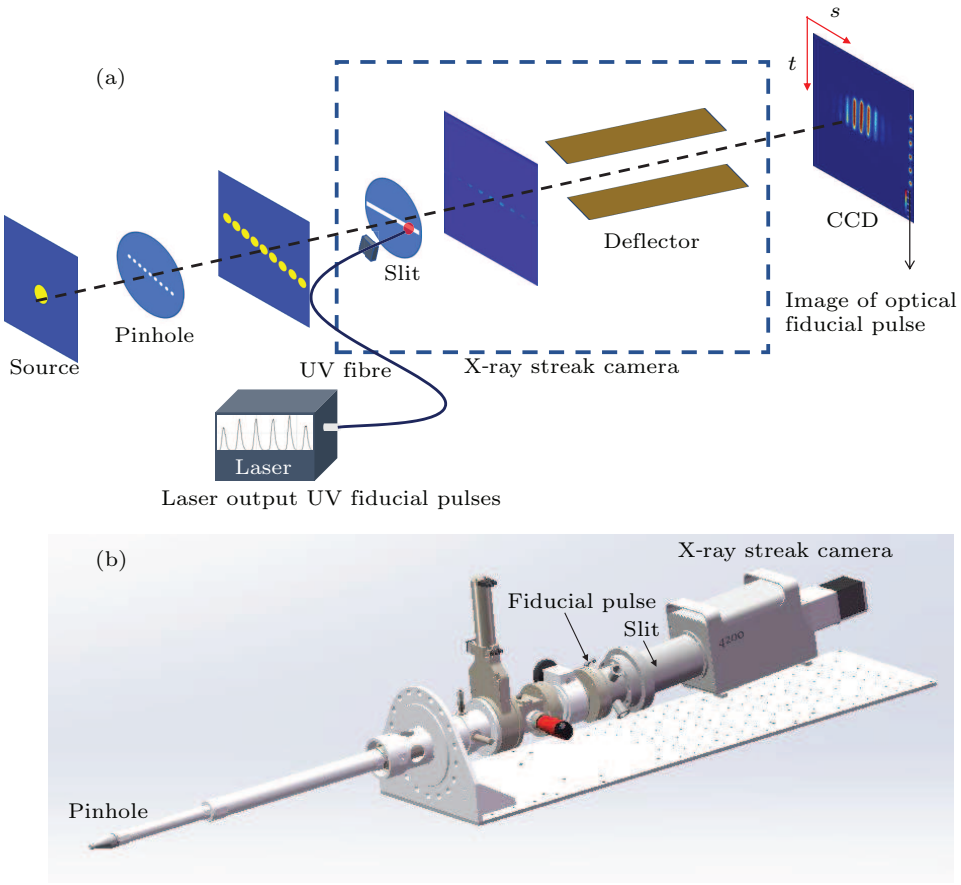


Fig. 1. (a) XSC combined with a pinhole array. The UV fiber is coupled from the slit to the XSC, and the intensity of the temporal fiducial pulses is enhanced by a ball lens and a 2D vacuum displacement platform. (b) Solid diagram of the MIXS-F system.

The principle of MIXS-F is illustrated in Fig. 2. A row of magnified images is formed on the slit of the XSC by a pinhole array tilted at an angle θ to the slit. The angle θ is determined based on factors, such as slit length, number of pinholes, magnification factor, and desired field of view. The source can be amplified into a row of the same size and slanted array through the pinhole array at an angle of θ to the slit, and it is sampled by the slit. In this way, the slit can simultaneously collect different areas of the same image and obtain the time evolution process of one-dimensional images at different positions of the source. The precise selection of θ ensures that the slit efficiently captures images without any loss or redundancy, safeguarding the integrity and authenticity of the reconstructed images throughout the process. At the same time, a sequence of temporal fiducial pulses is generated by a laser and transmitted to the slit end through an ultraviolet (UV) fiber, as shown in Fig. 2(a), serving as an additional time reference during experimental measurements. By precisely controlling the relative timing of the nanosecond (ns) laser and the temporal fiducial pulses, the ns laser's arrival time can be determined through the first pulse of the temporal fiducial pulses, which facilitates a more precise judgment of the collision moment after the end of the ns laser. This provides accurate heating time for subsequent injection of fast electrons. Furthermore, the temporal fiducial pulses also enable correction of the sweeping nonlinearity of the XSC. The nonlinearity

in scanning arises from fluctuations in the sweeping speed induced by the non-smooth slope voltage applied to the XSC. These variations in speed result in signal discrepancies across different positions within the imaging time window. The specific procedure for correcting the sweeping nonlinearity entails the following steps. First, temporal fiducial pulses are introduced, causing the fiber positioned at the slit's edge to emit quadruple-frequency light at a predetermined frequency. The scanning voltage drives this light to sweep across the detector with time, forming a sequence of evenly spaced light spots along the temporal axis. The interval between these light spots corresponds to the preset time interval between two luminous moments. By measuring the spacing between adjacent light spots throughout the entire image, the image can be processed accordingly. This method ensures temporal uniformity in the image dimension and effectively resolves the nonlinear issue caused by fluctuations in the scanning speed of XSC.

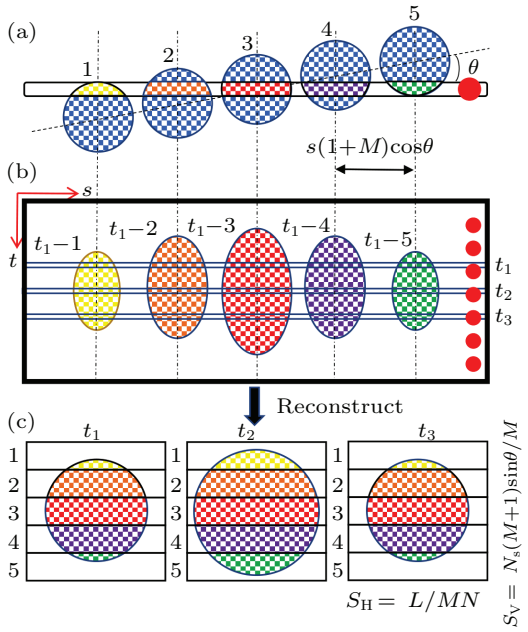


Fig. 2. Schematic diagram of MIXS-F. (a) The images acquired by a multi-pinhole array are cut by the slit with a tilting angle θ. (b) The streak images collected by XSC. (c) The reconstructed time-resolved 2D images.

The source passing through the pinhole array with magnification M is sampled at different positions in one dimension using the cathode slit to obtain a set of temporally resolved, one-dimensional images, as shown in Fig. 2(b). Thus, images of different positions of the source are separated by a constant vertical distance $s(M+1)\sin\theta/M$. Here, s is the separating distance between adjacent pinholes. These one-dimensional image sets are then sliced from left to right for each moment in time t_1, t_2, t_3, etc. The recombined images are then arranged from top to bottom, resulting in an ultrafast 2D structural evolution of the source, as shown in Fig. 2(c). Finally, the image smoothing technique is used to process the reconstructed image, and the high-quality 2D spatial evolution of plasma can be obtained. The separating distance $s > RM/(M+1)$ must be required. Here, R is the size of the source to avoid overlapping between images.

Meticulously adjusting the specifications of the MIXS-F solution ensures optimal performance, and researchers must take into account parameters, such as the angle θ, cathode slit length L, number of pinholes N, and magnification M, that limit the size of the field of view. The horizontal and vertical fields are defined as $S_{\rm H} = L/(MN)$ and $S_{\rm V} = N_{\rm s}(M+1)\sin\theta/M$, respectively. Additionally, the spatial resolution is influenced by the pinhole diameter D, slit width $d_{\rm k}$, and magnification M. In contrast, the temporal resolution is related to the time window and slit width $d_{\rm k}$. Ultimately, the number of framing can be as large as the streaked time divided by the temporal resolution of the streak camera.

Several advantages of the MIXS-F allow it to be excellent in ultrafast x-ray 2D imaging.[7] First, x-ray pinhole cameras and XSCs are already well established, making it easy to obtain fast 2D framing images. Second, the XSC not only can generate faster time-resolved images, but it can also acquire signals for prolonged periods by adjusting the time window as required, something that framed cameras cannot achieve. Third, the operating x-ray spectrum can be rather wide, ranging l–10 keV, which is determined by the filter and cathode materials. Finally, the laser time can be confirmed and the sweeping nonlinearity can be corrected by temporal fiducial pulses.

3. Design of MIXS-F

The material of the pinhole array is 10 μm thick tantalum, where the diameter of the pinhole is approximately 10 ± 1 μm and the spacing is 250 μm, with a total of 13 pinholes. Furthermore, four grooves 20 μm in width, 3 mm in length, and 5 μm in depth are also ablated by laser on the surface of the pinhole disk. These grooves are positioned facing the center pinhole to aid in their accurate positioning. Additionally, the horizontal grooves and the pinhole array are processed at a designed angle of 4.6° for optimal performance, as shown in Fig. 3. We use $s(1+1/M)\sin\theta$ as the sampling distance to cut the streak image.

The utilized XSC, model 4200, was manufactured by the Xi'an Institute of Optics and Precision Mechanics of the Chinese Academy of Sciences. The photocathode is cesium iodide (CsI) with a thickness of 150 nm, coated on an organic film. The horizontally placed slit has a length of 28 mm and a width of 100 μm. An optic scientific complementary metal-oxide semiconductor (sCOMS) with a resolution of 2048×2048 pixels was employed to record the image. The full time window was set to 5 ns.

To accurately determine the laser time and correct for the nonlinear sweeping speed, a UV fiber is coupled to the slit end.

However, the intensity of light influences the effectiveness of these pulses. To enhance the focus of the beam and improve the intensity of the temporal fiducial pulses obtained through the slit, a ball lens is added to the UV fiber. The ball lens causes the light beam to converge and increases light intensity by a factor of 1–4, significantly improving the quality of the temporal fiducial pulses. However, adding the ball lens alone is not enough to ensure precise calibration. Thus, a 2D vacuum displacement platform was installed to control the position of the UV fiber securely. This platform has a dual function: first, it can control the UV fiber's movement perpendicular to the slit, ensuring that the strongest part of the fiber is directly in the middle of the slit. Second, it controls the movement of the fiber toward or away from the slit, so that the focal point of the ball lens is located at the slit. These improvements work together to significantly increase the intensity of the temporal fiducial pulses by a factor of 50. Clearer temporal fiducial pulses help us to better determine the physical information by providing more accurate signals.

Through precise measurement of the relative delay between the ns laser and the temporal fiducial pulses, it has been determined that the time for the ns laser to reach the center of the target chamber is determined to be 350 ps later than the first pulse summit of the temporal fiducial pulses. The nonlinear effect of the sweeping speed is less than 3% and is rectifiable by utilizing the temporal fiducial pulses. Furthermore, trigger jitter performs well, generally better than 50 ps.

A combination of 200 nm Al and 10 μm Mylar was used as a filter to eliminate most low-energy stray light, and the system had sensitivity in the range of 1–10 keV. The pinhole array was placed at a distance of 200 mm from the target while maintaining a distance of 1435 mm between the pinhole array and the photocathode. The imaging system achieved a magnification ratio of $M = 7.2$.

Using a slit width of 100 μm and a time window of 5 ns, the temporal resolution attained by the experimental setup was 38 ps. However, improved temporal resolutions can be achieved by employing either shorter laser pulses or through the use of faster time windows.

The spatial resolution is determined by the pinhole diameter D, the streak camera slit width d_s, and the magnification M. The horizontal spatial resolution $\Delta r_x = (\Delta r_{PH}^2 + \Delta k_x^2)^{1/2}$, where Δr_{PH}^2 is the geometric resolution of the pinhole and $\Delta k_x = d_K/M$, where d_K is the spatial resolution of the slit. The vertical spatial resolution $\Delta r_y = (\Delta r_{PH}^2 + \Delta k_y^2)^{1/2}$, where $\Delta k_y = d_s/M$. $\Delta r_x = \Delta r_y = 18$ μm can be calculated. The basic system parameters are detailed in Table 1.

The aiming method is shown in Fig. 3. An internal-focusing telescope is employed to ensure accurate alignment of the slit of the XSC, pinhole, and target. First, the horizontal reference line of the telescope is aligned with the line connecting the slit and the center of the golden sphere. This is achieved by adjusting the attitude of the telescope. Subsequently, the center pinhole is adjusted to align with the center of the reference line. Finally, the pinhole array is rotated to align the four grooves with the reference line, thus ensuring that the slit is positioned at the specified angle of 4.6° to the pinhole array, and the center pinhole is aligned with the center of the slit and golden sphere. This process guarantees the precise alignment of the system for obtaining accurate results.

Table 1. MIXS-F system basic parameter index.

Magnification	$M = 7.2$
Number of pinholes	$N = 13$
Distance between pinholes	$S = 250$ μm
Pinhole array tilt angle	$\theta = 4.6°$
Slit length	$L = 28000$ μm
Slit width	$d_k = 100$ μm
Cathode material	CsI
Horizontal field of view	299 μm
Vertical field of view	296 μm
Horizontal spatial resolution	18 μm
Vertical spatial resolution	18 μm
Temporal resolution	38 ps

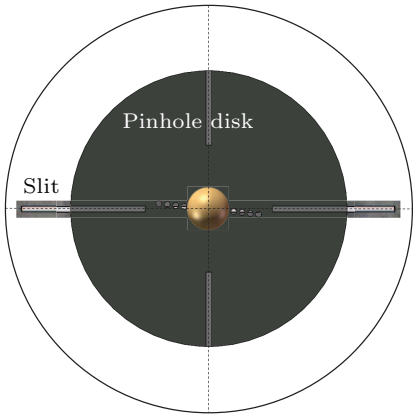


Fig. 3. View of the internal focusing telescope: aim at the center of the slit, pinhole, and golden sphere, and make the slit 4.6° from the pinhole array.

4. Experiment and result

The experiment was conducted at the SG-II laser facility at the National Laboratory on High Power Laser and Physics. Four drive lasers delivering a total energy of 1 kJ with 1 ns square pulse were directly focused onto the golden sphere center. The achieved average intensity is about 10^{15} W/cm^2 with the overlapped focal spot of about 150 μm at a wavelength of 351 nm. The configuration is depicted in Fig. 4.

Figure 5(a) shows the raw experimental results obtained from the XSC, where the temporal axis is the vertical direction and the spatial axis is horizontal. The results depict the time-sweep outcomes of signals gathered by 13 pinholes at different source locations. The visualization of edge results was achieved by enhancing contrast due to the significant intensity

difference between the center and edge intensities, leading to over saturation of the central intensity.

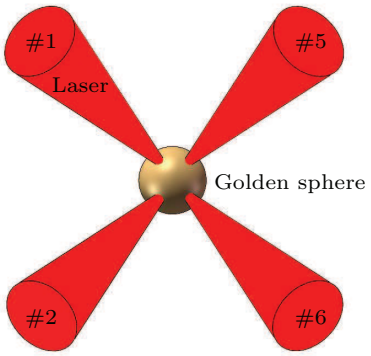


Fig. 4. Schematic diagram of the laser coupled with the golden sphere and the observation angle of diagnosis.

The circular spot on the right is the temporal fiducial pulses from the UV fiber corrected to the slit. It can be seen from the experimental results that through the optimization of the ball lens and the 2D vacuum displacement platform, the intensity of the temporal fiducial pulses is improved by about 50 times. Through measuring the temporal fiducial pulses, it is observed that the time interval between adjacent spots is 502 ps. The nonlinearity of the imaging region is subsequently obtained through examination of six light spots displayed by sCOMS. Through these adjustments, the image is corrected accordingly. Such precision measures and findings validate the efficacy of utilizing temporal fiducial pulses in the analysis and correction of XSC imaging. However, it is important to note that the circular imaging surface of the sCOMS results in the lower temporal fiducial pulses lying outside the field of view. Therefore, appropriate considerations should be taken into account when interpreting the results.

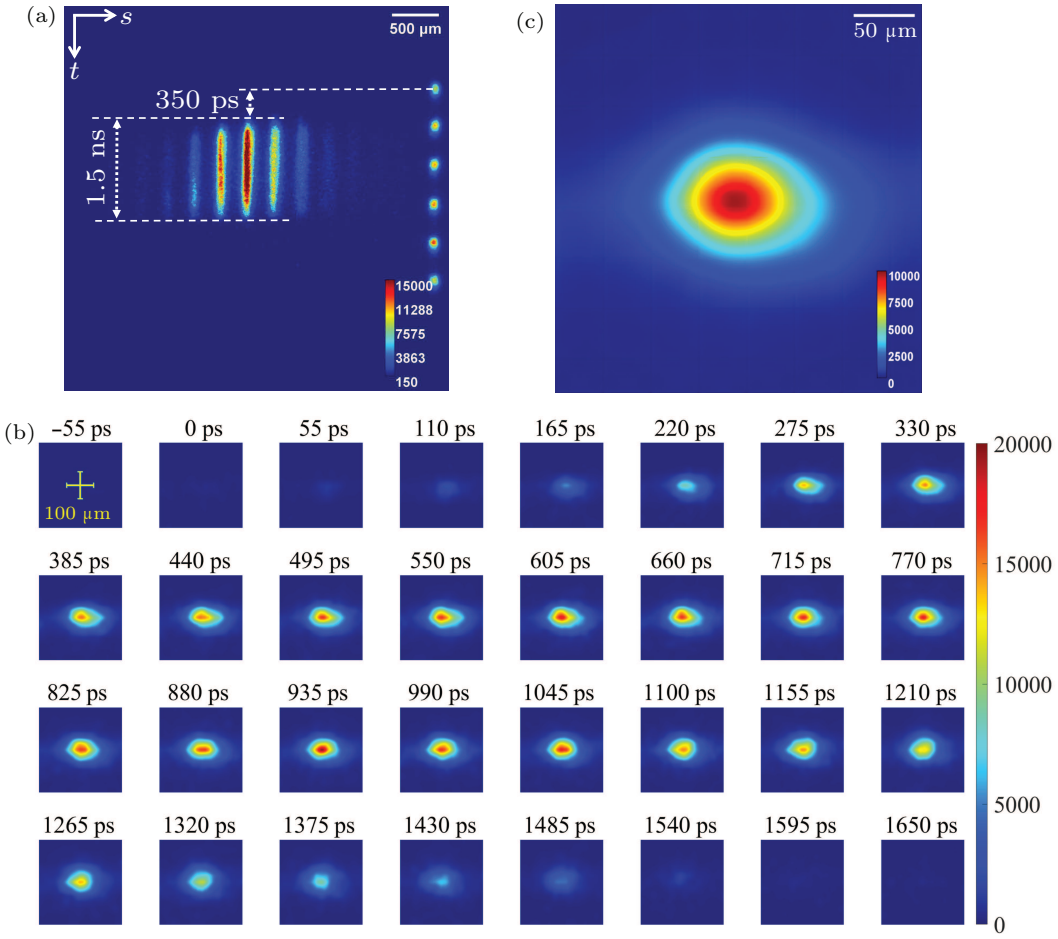


Fig. 5. (a) Streak camera results. (b) The evolution of the reconstructed 2D structure of the plasma. (c) Time integration result.

Using an image processing program to cut and reconstruct the streak image and then smoothing it, the evolution of the 2D structure of the plasma of the gold sphere is obtained, as shown in Fig. 5(b). The reconstructed results show that the whole plasma is elliptic, and this symmetry is suspected to be caused by the left and right laser energy imbalance, with 534 J and 556 J, respectively. The x-ray intensity starts to decrease from 1045 ps, which is caused by the laser pulse width being only 1 ns. As a result, the plasma luminescence weakens due to rapid radiation cooling after 1 ns. Figure 5(c) shows the time-integrated image, which can be seen to be still fairly uniform overall but lacks the more detailed structure shown in the time-resolved image.

The present results demonstrate the suitability of MIXS-F

for observing the rapid evolution of small-scale x-ray sources. This ultrafast x-ray 2D imaging technology enabled the detailed visualization of structural changes that are crucial for monitoring the inhomogeneity of the implosion process of ICF as well as the overall evolution of the current sheets during magnetic reconnection. In the future, we will apply the technique to the observation of the collision process of the double-cone collision ignition and the current sheets of magnetic reconnection.

5. Conclusions and perspectives

This work demonstrates the feasibility of multi-image x-ray fringe camera technology. A comprehensive 2D evolution of the plasma within the golden sphere is captured over time by utilizing an XSC with an elongated slit coupled with an array of 13 pinholes. Due to the elongated nature of the slit, employing multiple pinholes for sampling becomes viable, thereby enhancing the realism and level of detail in the reconstructed image. The inclusion of temporal fiducial pulses aids in accurate assessment of laser arrival time and facilitates correction of streak speed nonlinearity. The intensity of the temporal fiducial pulses sees a remarkable enhancement of approximately 50 times through the optimization of the ball lens and the implementation of a 2D vacuum displacement platform. An internally focused telescope is employed for monitoring and alignment purposes, while grooves on the pinhole disk, created via ultra-precision laser machining, assist in adjusting the angle between the slit and the pinhole array. By employing this optimization approach, experimental results with a temporal resolution of 38 ps and a spatial resolution of 18 μm are obtained. Future endeavors involve further optimization of the XSC, including shorter time windows and larger magnifications, to achieve finer temporal and spatial resolutions, with the ultimate goal of applying this technology in various physics experiments.

Acknowledgements

We are very grateful to the staff of the Shenguang laser facility in Shanghai and the researchers at Xi'an Institute of Optics and Precision Mechanics for their support of the use of the x-ray streak camera. This work was supported by the Strategic Priority Research Program of the Chinese Academy of Sciences (Grant Nos. XDA25030700 and XDA25030500), the National Key R&D Program of China (Grant Nos. 2022YFA1603200 and 2022YFA1603203), and the National Natural Science Foundation of China (Grant Nos. 12175018, 12135001, 12075030, and 11903006).

References

[1] Nuckolls J, Wood L, Thiessen A and Zimmerman G 1972 *Nature* **239** 139
[2] Heya M, Nakasuji M, Shiraga H, Miyanaga N, Azechi H, Takabe H, Yamanaka T and Mima K 1997 *Rev. Sci. Instrum.* **68** 820
[3] Bradley D K, Bell P M, Kilkenny J D, Hanks R, Landen O, Jaanimagi P A, McKenty P W and Verdon C P 1992 *Rev. Sci. Instrum.* **63** 4813
[4] Bradley D K, Bell P M, Landen O L, Kilkenny J D and Oertel J 1995 *Rev. Sci. Instrum.* **66** 716
[5] Shiraga H, Miyanaga N, Heya M, Nakasuji M, Aoki Y, Azechi H, Yamanaka T and Mima K 1997 *Rev. Sci. Instrum.* **68** 745
[6] Choi P and Aliaga R 1990 *Rev. Sci. Instrum.* **61** 2747
[7] Landen O L 1992 *Rev. Sci. Instrum.* **63** 5075
[8] Shiraga H, Heya M, Fujishima A, Maegawa O, Shimada K, Kato Y, Yamanaka T and Nakai S 1995 *Rev. Sci. Instrum.* **66** 722
[9] Shiraga H, Heya M, Fujioka S, Miyanaga N, Matsuoka M, Azechi H and Yamanaka T 2001 *Proceedings of SPIE* **4183** 339
[10] Zhong J, Shiraga H and Azechi H 2008 *Rev. Sci. Instrum.* **79** 396
[11] Tabak M, Hammer J, Glinsky M E, Kruer W L, Wilks S C, Woodworth J, Campbell E M, Perry M D and Mason R J 1994 *Phys. Plasmas* **1** 1626
[12] Zhang J, Wang W M, Yang X H, Wu D, Ma Y Y, Jiao J L, Zhang Z, Wu F Y, Yuan X H, Li Y T and Zhu J Q 2020 *Philos. T. R. Soc. A* **378** 20200015